



Contents lists available at ScienceDirect

## International Journal of Heat and Mass Transfer

journal homepage: [www.elsevier.com/locate/hmt](http://www.elsevier.com/locate/hmt)

# Near-junction phonon thermal spreading in GaN HEMTs: A comparative study of simulation techniques by full-band phonon Monte Carlo method

Yang Shen, Hong-Ao Yang, Bing-Yang Cao\*

Key laboratory of thermal science and power engineering of Education of Ministry, Department of Engineering Mechanics, Tsinghua University, Beijing 100084, China

## ARTICLE INFO

### Article history:

Received 26 March 2023

Revised 4 May 2023

Accepted 4 May 2023

### Keywords:

Ballistic transport

GaN high electron mobility transistor (HEMT)

Thermal spreading resistance

Phonon Monte Carlo (MC) simulation

## ABSTRACT

Accurate thermal simulation is essential for the near-junction thermal management and electro-thermal co-design of GaN HEMTs. While various methods have been employed to simulate phonon thermal transport in GaN, a comprehensive evaluation of their performance and reliability has yet to be conducted. In this work, first-principle-based steady-state full-band phonon tracing Monte Carlo (MC) simulations are conducted to study the thermal spreading resistance in GaN HEMTs. The results of full-band MC serve as a standard against which the applicability, accuracy, and computational efficiency of three widely-used approaches to simulate the near-junction phonon transport in GaN are thoroughly examined. The simulation techniques compared in this study include MC simulations with empirical isotropic phonon dispersion (isotropic MC), MC simulations with gray-medium approximation (gray MC), and finite-element methods (FEM) with effective thermal conductivities (FEM with  $k_{\text{eff}}$ ). It is found that isotropic MC largely overestimates the thermal resistance due to the empirical model's overestimation of phonon mean free path (MFP) distributions. By selecting an appropriate average MFP, gray MC can approximate the full-band results well, but due to its inability to reflect the contributions of different phonon modes, discrepancies are inevitable for some geometric parameters. For FEM-based analysis, although the diffusive nature of Fourier's law precludes the reproduction of channel temperature distributions, the influence of phonon ballistic effects on the junction temperature can be accurately reflected in the well-chosen effective thermal conductivities. The comparison highlights the importance of directly incorporating first-principles-calculated phonon properties into device thermal simulations, and the paper can provide a clearer understanding of near-junction thermal transport in GaN and can be useful for thermal simulations of GaN-based devices.

© 2023 Elsevier Ltd. All rights reserved.

## 1. Introduction

Gallium Nitride (GaN) high-electron-mobility transistors (HEMTs) are ideal for high-power and high-frequency applications [1–3], but the high power density in these devices can result in significant self-heating, undermining their performance and reliability [4–6]. Also, as device size continues to be miniaturized, thermal issues have become a bottleneck to fully exploit the electrical performance of GaN or other wide and ultra-wide bandgap devices [7–9]. This has resulted in a growing need for near-junction thermal management and electro-thermal co-design besides package-level cooling strategies [9–11]. To ensure optimal thermal designs and strike a balance between electrical and ther-

mal performance, it is crucial to understand the heat transport mechanism within the device and accurately predict the junction temperature under different design parameters and operating conditions [12–14].

In GaN HEMTs, heat is primarily generated at the top of the GaN layer and localized at the drain-side gate edge [15]. The width of the heat source can range from hundreds of nanometers to a few micrometers, depending on the bias voltage [16,17]. The area of the heat source is extremely small compared to the total device length and thickness, leading to a significant thermal spreading resistance that dominates the heat transport process in the HEMT [18,19]. Many efforts have been made to model the thermal spreading resistance using Fourier's law of heat conduction [20–23]. However, the main heat carriers in GaN are phonons whose mean free paths (MFPs) are comparable with the thickness of the GaN layer and the width of the heat generation area [24–26]. In

\* Corresponding author.

E-mail address: [caoby@tsinghua.edu.cn](mailto:caoby@tsinghua.edu.cn) (B.-Y. Cao).

this case, thermal transport is no longer diffusive and phonon ballistic effects can significantly increase the thermal resistance and raise the hotspot temperature [27,28]. Fourier's law becomes inapplicable in this scenario and Fourier's law-based thermal simulations may result in inaccurate thermal design rules and suboptimal trade-offs between electrical and thermal performance [7].

To account for the influence of phonon ballistic transport on the thermal spreading process, the phonon Boltzmann transport equation (BTE) should be solved in the near-junction region [29–31]. In theory, the most accurate simulation of the phonon transport process can be achieved by solving the full-band phonon BTE using first-principle-calculated phonon properties [32–34]. However, this can be computationally challenging and time-consuming due to the huge number of phonon states involved [35]. As a result, various substitutive methods have been generally employed in existing GaN-based device simulations. A common approach is to assume isotropic phonon properties and use an empirical phonon dispersion to replace the full-band phonon properties, which reduces the computation time by transforming the 3-D first Brillouin zone into a 1-D frequency space [13,36,37]. Some studies have also solved the gray-form BTE in the thermal simulations of GaN HEMTs [14,38]. The gray-medium approximation, in addition to the isotropy of phonon dispersion, further assumes that phonon properties are frequency-independent, thereby enabling the widespread phonon MFP distributions to be represented by an average MFP. Also, instead of solving the BTE, many studies use a size-dependent effective thermal conductivity to account for the influence of phonon ballistic effects [39,40]. The approach is easy to implement with finite element method (FEM)-based commercial software, and it is widely used in thermal analysis of GaN-based devices [18,41]. Though various methods have been adopted to reflect the influence of phonon ballistic transport on device temperatures, there has not been a thorough examination of the performance and reliability of the different approaches, making it challenging to utilize the results and findings from different studies. Thus, a comprehensive comparison between the different methods is necessary to more solidly cognize phonon thermal transport in GaN HEMTs.

In this study, first-principle-based steady-state full-band phonon tracing Monte Carlo (MC) simulations are conducted to investigate the thermal spreading resistance in GaN HEMTs. With the full-band predictions as a benchmark, the accuracy of different simulation techniques are evaluated under different geometric parameters, including (1) MC simulations with empirical isotropic phonon dispersion (Isotropic MC), (2) MC simulations with gray-medium approximation (Gray MC), and (3) FEM with effective thermal conductivities (FEM with  $k_{\text{eff}}$ ). Additionally, the computational efficiency of these methods for different geometric parameters is also examined. The comparison in the paper highlights the importance of directly incorporating first-principle-calculated phonon properties into device thermal simulations. This work could provide valuable insights for thermal simulations and the near-junction thermal designs for GaN HEMTs and similar devices.

## 2. Problem statement and methodologies

### 2.1. Problem statement

Figure 1 illustrates the simulation system of this study, which is a 2-D simplified model that represents the thermal spreading process of the GaN layer in a period of a multifinger HEMT [42]. The thickness of the GaN layer is denoted by  $t$ , and the width of one period is  $w$ . The c-axis (polarization axis) of GaN is aligned with the thickness direction, which is consistent with the fabrication process of most real devices. A uniform heat flux is modeled

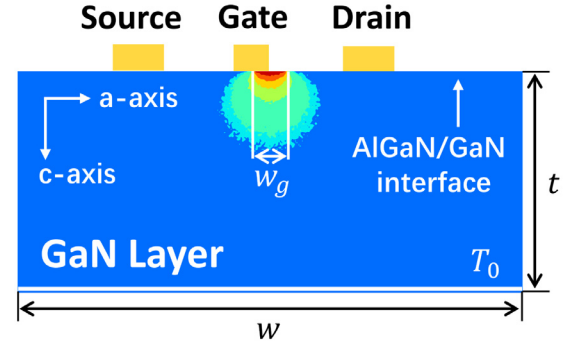


Fig. 1. Schematic of thermal spreading process of the GaN layer in GaN HEMTs.

at the top of the GaN layer to represent the heat source, with a width of  $w_g$  and a heating power of  $Q$ . As the non-uniform Joule heat distributions in the channel can be modeled as a combination of uniform heat sources with varying  $w_g$ , the results of the simplified model can be generalized to more complex electrothermal situations [13,15,16]. Since the focus of the comparison is on the thermal spreading resistance of the GaN layer, the substrate and interfacial thermal resistance are neglected in this study, thus the bottom boundary is set as an isothermal heat sink. The total thermal resistance,  $R_t$ , can be calculated using the mean heat source temperature ( $T_s$ ), the heat sink temperature ( $T_0$ ), and the total heating power ( $Q$ ),

$$R_t = \frac{\bar{T}_s - T_0}{Q}. \quad (1)$$

For ease of comparison, the dimensionless total thermal resistance can be introduced as  $R_t/R_{1d,0}$ , where  $R_{1d,0}$  is the 1-D thermal resistance under purely diffusive heat conduction,

$$R_{1d,0} = t/(wk_0), \quad (2)$$

where  $k_0$  is the bulk thermal conductivity.

### 2.2. Full-band phonon Monte Carlo simulation

Phonon dispersion and scattering rates in the full Brillouin zone are needed to drive the full-band phonon MC simulations. In this work, the phonon properties of wurtzite GaN are calculated using density functional theory (DFT) [43,44]. All DFT calculations are performed within the framework of the Vienna Ab initio Simulation Package (VASP) [45]. Projective augmented wave pseudopotential in Perdew–Burke–Ernzerhof formalism is employed for the exchange–correlation functional. Initially, the lattice constants of wurtzite GaN are optimized under symmetry constraints, and electronic self-consistent loops are terminated when the total free energy drop between successive steps is less than  $1 \times 10^{-7}$  eV. The ionic relaxation break condition is set such that the norms of all forces are smaller than  $1 \times 10^{-3}$  eV/Å. Second-order force constants are extracted from a  $4 \times 4 \times 3$  supercell with a  $\Gamma$ -centered  $4 \times 4 \times 3$   $k$  mesh using density functional perturbation theory. The Phonopy package is used to construct phonon dynamical matrices and calculate the phonon dispersion [46]. To compute the phonon scattering rate, third-order force constants within the five nearest neighbors are determined using the finite displacement method in DFT [47]. These force constants are then inputted into the ShengBTE package, which computes the three-phonon process scattering rates [48]. The resulting phonon dispersion and scattering rates for GaN are depicted in Fig. 2. The first Brillouin Zone is discretized into  $N$  wave vectors, with  $N = 15 \times 15 \times 15 = 3375$ . Since there are four atoms in a primitive cell, there are a total of 12 phonon branches, consisting of three acoustic branches and nine optical

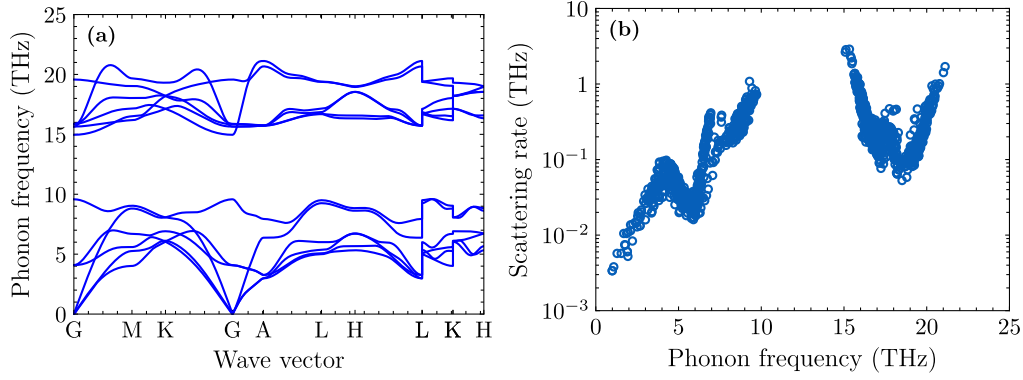


Fig. 2. First-principle-calculated phonon properties of GaN at 300 K. (a) Phonon dispersion along high symmetry points. (b) Phonon scattering rates.

branches. As a result, 40,500 available phonon states exist for MC simulations.

With the first-principle-calculated phonon states as inputs, full-band phonon Monte Carlo (MC) simulations can be initiated to simulate phonon transport. This study adopts the steady-state phonon tracing MC simulations [49,50] as opposed to ensemble implementations that are naturally in a transient scheme to reduce computation time. In phonon tracing MC simulations, each phonon bundle represents a fixed amount of power and all contributions to phonon movements contribute to the accumulation of temperatures. The variance-reduced technique is also employed in the MC simulations to further improve computational efficiency, i.e. only variations from the reference equilibrium state are counted [51,52]. In the thermal spreading process depicted in Fig. 1, the phonon bundle originates from the heat flux boundary, undergoes drift and scatter events in the domain, and is eventually absorbed by the bottom isothermal heat sink. The properties of emitted and scattered phonon bundles are drawn from the first-principle-calculated phonon states, with weights determined according to different criteria. In phonon emission process, the number of emitted phonon bundles of a boundary with temperature  $T_b$  can be expressed as

$$N(T_b) = \frac{1}{\epsilon_{\text{eff}} V} \sum_{\text{state } j} \vec{v}_j \cdot \vec{n} \hbar \omega_j [f_{\text{BE}}(\omega_j, T_b) - f_{\text{BE}}(\omega_j, T_{\text{ref}})], \vec{v}_j \cdot \vec{n} > 0, \quad (3)$$

where  $\epsilon_{\text{eff}}$  is the power represented by a phonon bundle,  $V$  is the volume of the primitive cell,  $\vec{v}_j$  is the group velocity,  $\vec{n}$  is the normal vector of the boundary,  $f_{\text{BE}}(\omega, T) = \frac{1}{\exp(\hbar\omega/k_B T) - 1}$  is the Bose-Einstein distribution, and  $T_{\text{ref}}$  is the selected reference temperature. The mode of emitted phonons is drawn with probabilities propor-

tional to  $\vec{v}_j \cdot \vec{n} \hbar \omega [f_{\text{BE}}(\omega_k, T_b) - f_{\text{BE}}(\omega_k, T_{\text{ref}})]$ . The emitted phonon bundle undergoes free flight until a scattering event occurs. The flight distance before scattering is drawn as  $\vec{l} = -\vec{v}_j \tau_j \ln(R_l)$ , where  $R_l$  is a uniform random number in [0,1] and  $\tau_j$  is the relaxation time. After scattering, the phonon mode is redrawn with probabilities proportional to  $\hbar \omega [f_{\text{BE}}(\omega_k, T_{\text{loc}}) - f_{\text{BE}}(\omega_k, T_{\text{ref}})] / \tau_k$ , and the process of drift and scatter repeats until the phonon bundle is absorbed by an isothermal boundary. In the case of a collision with an adiabatic boundary, the phonon bundle is diffusively scattered to its iso-energy state. The probability of drawing the  $j$ -mode phonon is proportional to  $(\vec{v}_j \cdot \vec{n}) \delta(\omega - \omega_{\text{in}})$ ,  $\vec{v}_j \cdot \vec{n} > 0$ . Due to the discrete nature of phonon states, strict energy conservation is relaxed to frequency variations smaller than a discretization step  $\Delta\omega$  [53]. In this study,  $\Delta\omega$  is set to  $\Delta\omega = \omega_m/100$ , where  $\omega_m$  is the maximum phonon frequency in GaN, and it has been verified that this choice does not affect the simulation results. By simulating a sufficient number of phonon bundles, the statistical error is reduced to an acceptable level, and temperature distributions can be extracted from the phonon distributions.

Two benchmark simulations, investigating cross-plane and in-plane heat conduction in GaN films, are conducted to validate the developed full-band phonon tracing Monte Carlo (MC) simulations. In both cases, the film is heated by two heat sinks with different temperatures. The thickness in the direction of the temperature difference is represented by  $L_x$ , while the lateral distance is represented by  $L_y$ . In cross-plane heat conduction, the lateral boundaries are periodic, and the effective thermal conductivity of the film is controlled by  $L_x$ . In in-plane heat conduction,  $L_x$  is set to be large enough to eliminate the  $x$ -directional size effect, and the effective thermal conductivity is instead controlled by  $L_y$ . Figure 3 illustrates the ratios of the effective thermal conductivity to the bulk value

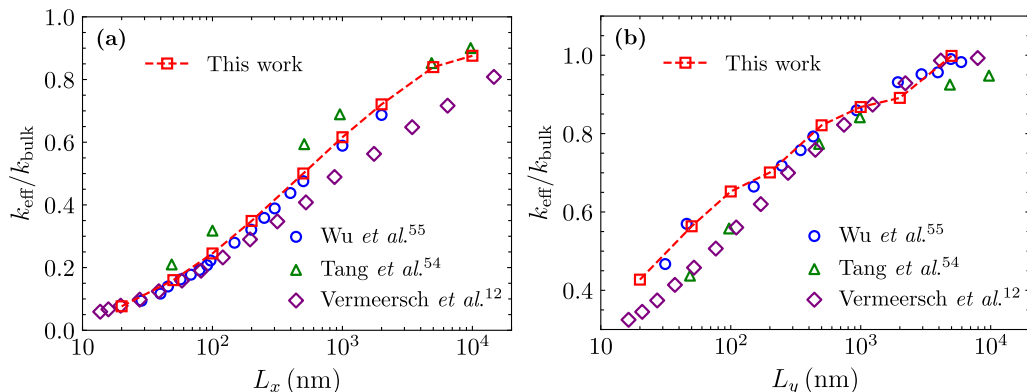


Fig. 3. Effective thermal conductivity varying with the characteristic length in (a) cross-plane heat conduction and (b) in-plane heat conduction.

**Table 1**  
Fitted phonon dispersion and relaxation time parameters for GaN.

$k_0 (1 \times 10^9 \text{ m}^{-1})$	$\omega_m (1 \times 10^{13} \text{ rad/s})$	$a_D (\text{Å})$	$A (1 \times 10^{-45} \text{ s}^3)$	$B (1 \times 10^{-19} \text{ s/K})$	$C (\text{K})$
10.94	3.50	2.87	5.26	1.10	200

as a function of the characteristic length. Literature results are also given for comparison, including the model-predicted values from Tang et al. [54], and the numerical values from Wu et al. [55] and Vermeersch et al. [12]. It can be observed that the MC simulations successfully capture the features of ballistic-diffusive heat conduction, with the results being in good agreement with the reference values.

### 2.3. Substitutive simulation methods

With the full-band predictions as a benchmark, three substitutive simulation methods are compared including isotropic MC, gray MC, and FEM with  $k_{\text{eff}}$ . In isotropic MC, phonon properties are assumed to be isotropic and dependent only on phonon frequencies and phonon branches. As a result, phonon modes can be drawn from the one-dimensional frequency space rather than the three-dimensional first Brillouin zone, which reduces computation time a lot. For phonon simulations in GaN HEMTs, the commonly used phonon dispersion model is the sine-shaped Born-von Karman dispersion [13,29]. In this model, the relationship between the angular frequency  $\omega$  and wave vector  $k$  can be expressed as  $\omega(k) = \omega_m \sin(\pi k/2k_m)$ , where  $k_m = (6\pi^2 n)^{1/3}$  and  $n$  is the volumetric density of primitive cells. The relaxation time can be depicted as  $\tau^{-1} = \tau_I^{-1} + \tau_U^{-1} = A\omega^4 + B\omega^2 T \exp(-C/T)$ , where  $\tau_I$  represents impurity scattering and  $\tau_U$  represents Umklapp phonon-phonon scattering [56]. The constants  $A$ ,  $B$ , and  $C$  are dependent on the material and can be determined by fitting the bulk thermal conductivities as a function of temperature. For GaN, the fitted phonon dispersion and relaxation time parameters are shown in Table 1.

Figure 4 (a) illustrates the bulk thermal conductivity of GaN along the c-axis as a function of temperature, as predicted by first-principle calculations and the empirical model. The empirical model with the fitted parameters is capable of accurately reflecting the temperature dependence of the thermal conductivity of GaN. However, as demonstrated in Fig. 4(b), the empirical model exhibits an overestimation of the phonon MFP distributions. The first-principle calculations indicate that at 300 K, phonons with MFPs less than 300 nm contribute to 50% of the bulk thermal conductivity, while the corresponding value for the empirical model is 1000 nm. This overestimation can be attributed to the empirical phonon dispersion's inability to properly reflect the density of

states of GaN. Thus, for the best fitting of bulk thermal conductivity, there is a large deviation for MFP distributions.

In gray MC, in addition to assuming isotropy, phonon properties are further assumed to be frequency-independent, and an average phonon mean free path (MFP) is used to represent the entire phonon spectrum [57]. In this case, the properties of the simulated phonon bundle remain unchanged, and only the direction of movement needs to be resampled during the simulation [50]. This approximation enables fast numerical analysis of phonon ballistic effects, whereas the accuracy strongly depends on the choice of the representative MFP [14,38]. Li et al. [57] compared different methods for calculating the average MFP and found that extracting the average MFP from the fitting of size-dependent effective thermal conductivities well reflects the phonon ballistic effects. By employing Majumdar's model for cross-plane heat conduction to calculate the effective thermal conductivity [58] and minimizing  $\mathcal{L}(l_{\text{ave}})$ , where

$$\mathcal{L}(l_{\text{ave}}) = \sum_t \left| \frac{1}{3} \sum_j \int_0^{\omega_j} \frac{\hbar \omega \frac{\partial f_0}{\partial T} \text{DOS}_j(\omega) v_{g,j} l_j}{1 + \frac{4}{3} \frac{l_j}{t}} d\omega - \frac{1}{1 + \frac{4}{3} \frac{l_{\text{ave}}}{t}} \right|^2, \quad (4)$$

the average MFP  $l_{\text{ave}}$  can be determined. The fitted average MFP for the phonon properties of GaN calculated in this work is equal to 300 nm.

As an alternative approach that is easy to integrate with FEM-based thermal analysis, the impact of phonon ballistic effects can be reflected by effective thermal conductivity. Although the temperature field cannot be fully reconstructed due to the diffusive nature of Fourier's law, FEM-based analysis can predict a junction temperature similar to the one obtained from BTE-based simulations, given a reasonable value for effective thermal conductivity. Previous studies have established a semi-empirical effective thermal conductivity model for thermal spreading process in a ballistic-diffusive regime, based on phonon BTE and isotropic MC simulations [42,59],

$$k_{\text{eff}} = \frac{1}{3} \sum_j \int_0^{\omega_j} \hbar \omega \frac{\partial f_0}{\partial T} \text{DOS}_j(\omega) v_{g,\omega,j} l_{m,j} d\omega \quad (5)$$

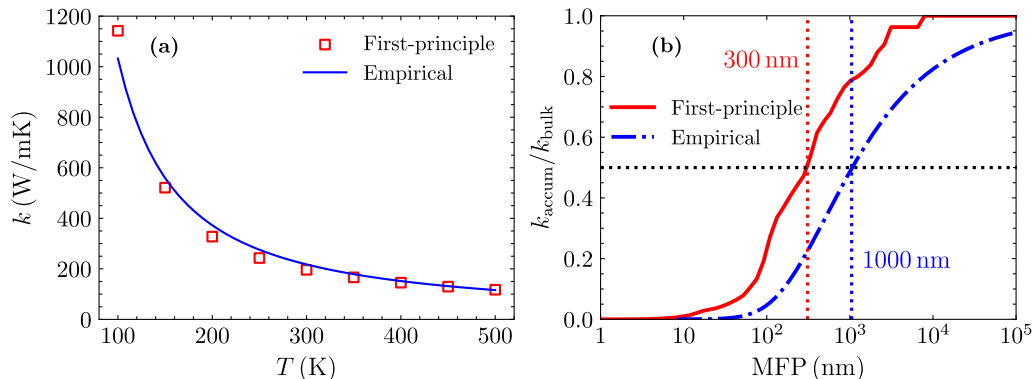


**Fig. 4.** Comparison between first-principle-based predictions and the empirical model for GaN. (a) Bulk thermal conductivity varying with temperature along c axis. (b) Thermal conductivity accumulation function at 300 K.

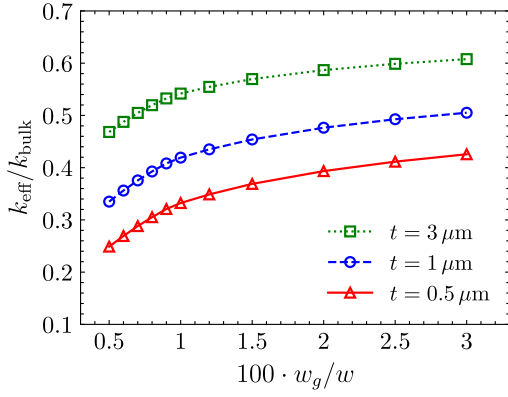


Fig. 5. Model-predicted effective thermal conductivities as a function of  $w_g/w$ , with  $w/t = 20$ .

where

$$l_{m,j} = \frac{l_{0,j}}{\left(1 + \frac{2}{3}Kn_{t,\omega,j}\right)\left(1 + A_w\left(\frac{w_g}{w}, \frac{w}{t}\right)Kn_{w,\omega,j}\right)r_t r_{wg}} \quad (6)$$

In this model,  $l_{0,j}$  is the intrinsic frequency-dependent MFP of the  $j$  branch phonon, and  $Kn_{t,\omega,j} = l_{0,j}/t$  and  $Kn_{w,\omega,j} = l_{0,j}/w_g$  are phonon Knudsen numbers, where  $t$  is the thickness of the GaN layer and  $w_g$  is the width of the heat source. The terms  $1 + 2/3Kn_{t,\omega,j}$  and  $r_t$  are used to account for the cross-plane ballistic effect, and  $1 + A_wKn_{w,\omega,j}$  and  $r_w$  are used to consider the ballistic effect resulting from a heat source size comparable to the MFPs. The details on the model can be found in Refs. [42] and [59]. Figure 5 shows the model-predicted effective thermal conductivities of GaN, as a function of  $w_g/w$ , for different values of

$t$ . Both the cross-plane ballistic effect and the heat source size-induced ballistic effect are captured by the effective thermal conductivities. As  $t$  and  $w_g/w$  decrease, the effective thermal conductivity decreases significantly compared to its bulk value.

### 3. Results and discussion

Figure 6 displays the dimensionless total thermal resistance predicted by various methods. The simulations are performed for systems with different geometric parameters, with the selected parameter range encompassing most of the design space for GaN HEMTs. The results obtained from the different approaches are significantly higher than those predicted using bulk thermal conductivities, highlighting the importance of carefully considering phonon ballistic effects in device thermal simulations. It should be noted that in this work the bottom boundary of the GaN layer is set as isothermal, thus the total thermal resistance here is only used to characterize the thermal resistance of the GaN layer instead of the total device. Compared with the previous work that focuses on the absolute temperature [14,29,38], the thermal resistance defined here can more clearly illustrate the influence of the phonon ballistic effects [13,30,42,59]. Among these methods, the thermal resistance predicted by isotropic MC is significantly higher than the full-band predictions with all geometric parameters, which can be attributed to the longer phonon MFPs calculated by the empirical phonon property model. It implies that the previous MC simulations based on the empirical model may overestimate the hotspot temperature in GaN HEMTs [13,29,36,37,59]. However, despite the discrepancy in values, the thermal resistance predicted by isotropic MC has a nearly identical curve shape to the full-band results due to the similar shape of the phonon MFP spectrum as shown in Fig. 4(b).

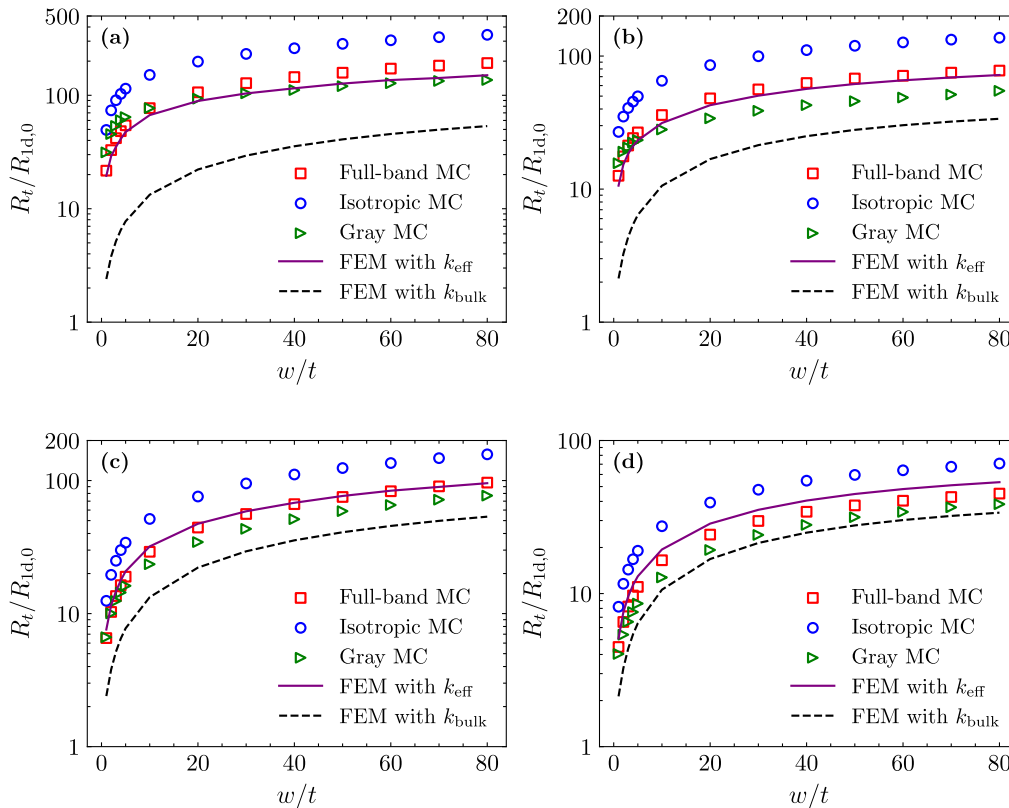


Fig. 6. Dimensionless total thermal resistance as a function of  $w/t$  with (a)  $t = 0.5 \mu\text{m}$ ,  $w_g/w = 0.005$ , (b)  $t = 0.5 \mu\text{m}$ ,  $w_g/w = 0.02$ , (c)  $t = 3 \mu\text{m}$ ,  $w_g/w = 0.005$ , and (d)  $t = 3 \mu\text{m}$ ,  $w_g/w = 0.02$ .

In the case of gray MC, the predicted thermal resistance is very similar to the full-band predictions, suggesting that by choosing an appropriate average phonon MFP, the gray-medium approximation can effectively reflect the influence of phonon ballistic effects. However, as shown in Fig. 6(a), it can be seen that gray MC simulations cannot completely reproduce the full-band results. When  $w/t$  is small, the gray MC-predicted thermal resistance is higher than the full-band predictions, whereas when  $w/t$  is large, the gray MC predictions get lower instead. This discrepancy illustrates the intrinsic limitation of the gray-medium approximation in reflecting the contributions of different phonon modes. The comparison between isotropic MC using empirical phonon dispersion and gray MC also suggests that, more precise temperature predictions can be obtained by combining isotropic MC with frequency-averaged first-principle-calculated phonon properties, since both the accurate phonon properties and the influence of phonon MFP spread can be taken into account. For FEM with  $k_{\text{eff}}$ , the predictions are always in good agreement with the full-band results, with all the geometric parameters considered in this work. This indicates that the influence of phonon ballistic effects on the device junction temperature can be well reflected by using effective thermal conductivities. Also, the effective thermal conductivity model, which is developed using isotropic phonon dispersion, is still valid for first-principle-calculated phonon properties, given the similar shape of the MFP spectrum and the weak anisotropy of GaN above room temperature [59].

Among the different methods, gray MC and FEM with  $k_{\text{eff}}$  can relatively well approximate the full-band results, since the first-principle-calculated phonon properties are directly used as model inputs, i.e. calculating the average MFP and size-dependent effective thermal conductivities. Isotropic MC has the lowest accuracy since the used empirical phonon properties are determined by fitting the bulk thermal conductivities, instead of being obtained from the first-principle-predicted phonon properties. This comparison emphasizes the importance of directly incorporating first-principles-calculated phonon properties into device thermal simulations, no matter what kind of simulation technique is adopted.

The total thermal resistance of thermal spreading process in a ballistic-diffusive regime can be attributed to three effects: (1) the thermal spreading effect, (2) the cross-plane ballistic effect related to the film thickness, and (3) the ballistic effect with the heat source size comparable with MFP. To better understand the reliability of different methods for devices with different geometric parameters, it is meaningful to examine the different ballistic effects separately. The 1-D thermal resistance, which eliminates the influence of thermal spreading effect and the heat source size-induced ballistic effect in the average of temperatures, can be used to measure the strength of the cross-plane ballistic effect. As shown in Fig. 7, the dimensionless 1-D thermal resistance predicted by different methods is plotted as a function of  $t$ . The isotropic MC predicted 1-D thermal resistance is significantly higher than the full-band results, which highlights the strong relationship between the phonon spectrum and the cross-plane ballistic effect caused by phonon-boundary scattering. The results predicted by gray MC and FEM with  $k_{\text{eff}}$  are in good agreement with the full-band predictions, despite some minor differences. Gray MC slightly underestimates the 1-D thermal resistance when  $t$  is small and the cross-plane ballistic effect strong. FEM with  $k_{\text{eff}}$  overestimates the 1-D thermal resistance when  $t$  is large, and overestimates when  $t$  is relatively small, since there are fitting parameters in the effective thermal conductivity model trying to minimize the overall deviations for various geometric parameters and materials [59]. The comparison between different methods further suggests the importance of properly treating phonon properties before simulations.

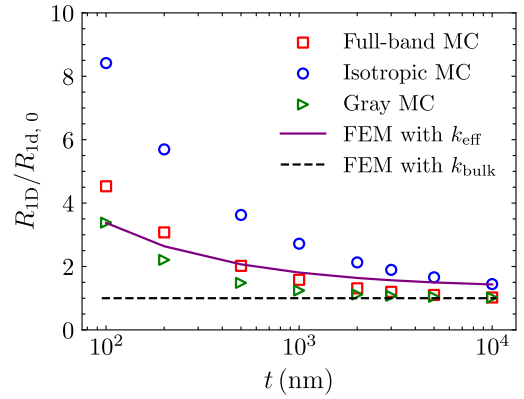


Fig. 7. Dimensionless 1-D thermal resistance varying with  $t$ .

To evaluate the heat source size-induced ballistic effect, a thermal resistance ratio  $r_w$  can be defined as  $r_w = \frac{R_t/R_{1D}}{R_{t,k,\text{bulk}}/R_{1D,0}}$ , where  $R_{t,k,\text{bulk}}$  represents the total thermal resistance calculated with FEM using the bulk thermal conductivity. The thermal spreading effect and cross-plane ballistic effect are cancelled out in this ratio, and  $r_w$  serves as a reflection of the ballistic effect with  $w_g$  comparable to MFP. Figure 8 shows the thermal resistance ratio  $r_w$  as a function of  $w_g$  with different  $w/t$ . Except for the bulk values,  $r_w$  increases as  $w_g$  decreases, which is attributed to the enhanced phonon ballistic transport. Previous electrothermal simulations have indicated that for devices working in saturation regime, the Joule heat is concentrated at the drain-side gate edge with a width of approximately 160 nm [13,15,16]. It is emphasized the importance of carefully considering the heat source-related ballistic effect in order to accurately predict the hotspot temperature. As shown in Fig. 8, in contrast to the 1-D thermal resistance, the differences in  $r_w$  predicted by different methods are not too significant. However, the isotropic MC predictions are still higher than the full-band results due to the overestimation of phonon MFP spectrum. The gray MC-predicted  $r_w$  are generally lower than the full-band results and increase more quickly with  $w_g$  decreasing, since the influence of phonon MFP distributions can not be well considered. FEM with  $k_{\text{eff}}$  can still approximately depict the  $w_g$  dependence of  $r_w$ , but its accuracy decreases rapidly with the decrease of  $w_g$  due to the declined reliability of the model with enhanced phonon ballistic transport.

Figure 9 compares the computation time of different simulation methods as a function of the system thickness  $t$ . Full-band MC, which considers a large number of phonon states is the most computationally demanding among the all the methods. With the simplification of phonon dispersion, the computation time of isotropic MC is reduced by 1 ~ 2 orders of magnitude compared to full-band MC. Gray MC, which replaces the entire phonon spectrum with an average MFP, further reduces computation time by nearly another order of magnitude compared to isotropic MC. In contrast to BTE-based approaches, FEM-based simulations have computation time that is far lower and nearly independent of the system size. While Fourier's law-based simulations may not provide accurate predictions of channel temperature distributions, FEM-based analysis using an appropriate  $k_{\text{eff}}$  can offer efficient estimations of junction temperature for different geometric parameters. However, to obtain the most accurate temperature field for the entire device, it is essential to develop a multiscale simulation framework that combines first-principle calculations, phonon BTE, and FEM simulations [12,30]. The coupling between heat generation and phonon transport should also be thoroughly considered to achieve self-consistent electrothermal simulations and investigate the thermal effects on the device electrical performance

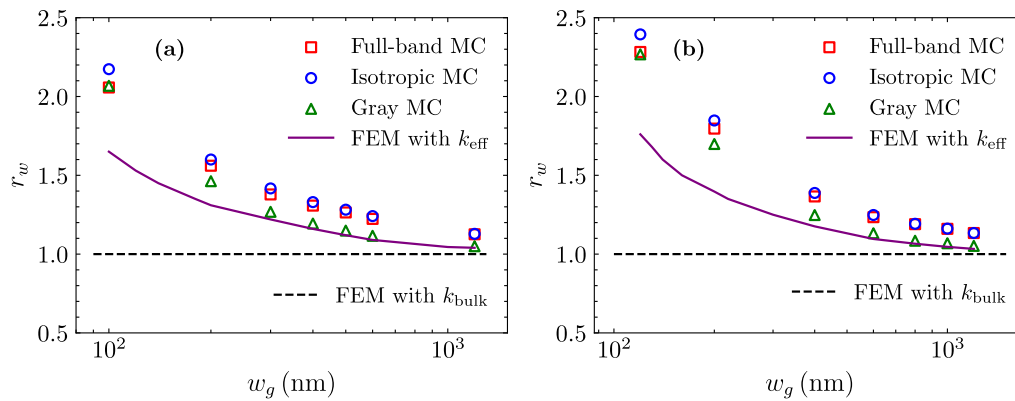


Fig. 8. Thermal resistance ratio  $r_w$  as a function of  $w_g$ , with (a)  $w/t = 20$ , and (b)  $w/t = 40$ ,  $t = 1 \mu\text{m}$ .

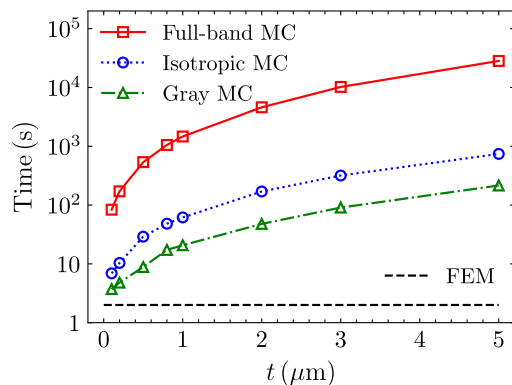


Fig. 9. Computation time as a function of  $t$ , with  $w/t = 40$ ,  $w_g/w = 0.01$ . The phonon number is chosen as  $10^6$ , which guarantees the convergence after verification. All the simulations are coded in Python with Numba and carried out with a single processor on Apple M1 Pro chip.

[36,37]. Additionally, high-resolution experimental techniques are necessary to characterize the device hotspots and validate the simulation models [14,60–62].

#### 4. Conclusion

In this paper, the first-principle-based full-band phonon MC simulations are conducted to investigate the thermal spreading resistance in GaN HEMTs. Three widely used simulation methods, including (1) isotropic MC, (2) gray MC, and (3) FEM with  $k_{\text{eff}}$ , are compared against the full-band MC results to examine their performance. It is found that isotropic MC largely overestimates the thermal resistance due to the empirical model's overestimation of MFP distributions. However, the predicted thermal resistance variation tendency is nearly identical to the full-band results, since the contributions of phonons with different MFPs can be considered in the simulation, and the shape of the MFP spectrum predicted by the empirical model is similar to the first-principle predictions. Gray MC can approximate the full-band predictions by selecting an appropriate average MFP, but cannot completely reproduce the results for all geometric parameters due to its limitation in considering the wide spread of phonon MFPs. The predictions of FEM with  $k_{\text{eff}}$  show good consistency with the full-band results for various geometric parameters, and the computation time is several orders of magnitude lower and nearly independent of the system size compared to the BTE-based simulations. Although the Fourier's law-based simulation can not accurately reconstruct the temperature field, it can still be used as a fast and effective ap-

proach for junction temperature predictions to guide device thermal designs. The comparison highlights the importance of directly incorporating first-principles-calculated phonon properties into device thermal simulations, no matter what kind of simulation technique is adopted. This paper provides a comprehensive comparison of different simulation methods for the thermal spreading process in GaN, and the results and analysis could be useful for thermal simulations of GaN HEMTs or HEMT-like devices.

#### Declaration of Competing Interest

The authors declare that they have no known competing financial interests or personal relationships that could have appeared to influence the work reported in this paper.

#### CRediT authorship contribution statement

**Yang Shen:** Conceptualization, Data curation, Formal analysis, Investigation, Methodology, Software, Validation, Visualization, Writing – original draft. **Hong-Ao Yang:** Investigation, Methodology, Software, Writing – original draft. **Bing-Yang Cao:** Conceptualization, Funding acquisition, Project administration, Supervision, Writing – review & editing.

#### Data availability

No data was used for the research described in the article.

#### Acknowledgment

This work was supported by the National Natural Science Foundation of China under Grants 51825601 and U20A20301.

#### References

- [1] M. Meneghini, C. De Santi, I. Abid, M. Buffolo, M. Cioni, R.A. Khadar, L. Nela, N. Zagni, A. Chini, F. Medjdoub, et al., GaN-based power devices: physics, reliability, and perspectives, *J. Appl. Phys.* 130 (18) (2021) 181101.
- [2] M. Haziq, S. Falina, A.A. Manaf, H. Kawarada, M. Syamsul, Challenges and opportunities for high-power and high-frequency AlGaIn/GaN high-electron-mobility transistor (HEMT) applications: a review, *Micromachines* 13 (12) (2022) 2133.
- [3] K.H. Hamza, D. Nirmal, A review of GaN HEMT broadband power amplifiers, *AEU-Int. J. Electron. Commun.* 116 (2020) 153040.
- [4] M. Rosker, C. Bozada, H. Dietrich, A. Hung, D. Via, S. Binari, E. Vivierios, E. Cohen, J. Hodiak, The DARPA wide band gap semiconductor for RF applications (WBGS-RF) program: phase II results, *CS ManTech* 1 (2009) 1–4.
- [5] B. Padmanabhan, D. Vasilevka, S.M. Goodnick, Reliability concerns due to self-heating effects in GaN HEMTs, *J. Integr. Circuits Syst.* 8 (2) (2013) 78–82.
- [6] K. Ranjan, S. Arulkumar, G.I. Ng, A. Sandupatla, Investigation of self-heating effect on DC and RF performances in AlGaIn/GaN HEMTs on CVD-diamond, *IEEE J. Electron. Devices Soc.* 7 (2019) 1264–1269.

- [7] S. Choi, S. Graham, S. Chowdhury, E.R. Heller, M.J. Tadjer, G. Moreno, S. Narumanchi, A perspective on the electro-thermal co-design of ultra-wide bandgap lateral devices, *Appl. Phys. Lett.* 119 (17) (2021) 170501.
- [8] R.J. Warzoha, A.A. Wilson, B.F. Donovan, N. Donmez, A. Giri, P.E. Hopkins, S. Choi, D. Pahinkar, J. Shi, S. Graham, et al., Applications and impacts of nanoscale thermal transport in electronics packaging, *J. Electron. Packag.* 143 (2) (2021).
- [9] Y. Qin, B. Albano, J. Spencer, J.S. Lundh, B. Wang, C. Buttay, M.J. Tadjer, C. Di-Marino, Y. Zhang, Thermal management and packaging of wide and ultra-wide bandgap power devices: a review and perspective, *J. Phys. D* 56 (9) (2023) 093001.
- [10] B. Chatterjee, D. Ji, A. Agarwal, S.H. Chan, S. Chowdhury, S. Choi, Electro-thermal investigation of GaN vertical trench MOSFETs, *IEEE Electron. Device Lett.* 42 (5) (2021) 723–726.
- [11] B. Wang, M. Xiao, Z. Zhang, Y. Wang, Y. Qin, Q. Song, G.-Q. Lu, K. Ngo, Y. Zhang, Chip size minimization for wide and ultrawide bandgap power devices, *IEEE Trans. Electron. Devices* 70 (2) (2023) 633–639.
- [12] B. Vermeersch, R. Rodriguez, A. Sibaja-Hernandez, A. Vais, S. Yadav, B. Parvais, N. Collaert, Thermal modelling of GaN & InP RF devices with intrinsic account for nanoscale transport effects, in: 2022 International Electron Devices Meeting (IEDM), IEEE, 2022, pp. 15–23.
- [13] Y. Shen, X.-S. Chen, Y.-C. Hua, H.-L. Li, L. Wei, B.-Y. Cao, Bias dependence of non-fourier heat spreading in GaNHEMTs, *IEEE Trans. Electron. Devices* 70 (2) (2022) 409–417.
- [14] B. Chatterjee, C. Dundar, T.E. Beechem, E. Heller, D. Kendig, H. Kim, N. Donmez, S. Choi, Nanoscale electro-thermal interactions in AlGaN/GaN high electron mobility transistors, *J. Appl. Phys.* 127 (4) (2020) 044502.
- [15] X. Chen, S. Boumaiza, L. Wei, Self-heating and equivalent channel temperature in short gate length GaN HEMTs, *IEEE Trans. Electron. Devices* 66 (9) (2019) 3748–3755.
- [16] X. Chen, S. Boumaiza, L. Wei, Modeling bias dependence of self-heating in GaN HEMTs using two heat sources, *IEEE Trans. Electron. Devices* 67 (8) (2020) 3082–3087.
- [17] R. Pearson, B. Chatterjee, S. Kim, S. Graham, A. Rattner, S. Choi, Guidelines for reduced-order thermal modeling of multifinger GaN HEMTs, *J. Electron. Packag.* 142 (2) (2020) 021012.
- [18] C. Song, J. Kim, J. Cho, The effect of GaN epilayer thickness on the near-junction thermal resistance of GaN-on-diamond devices, *Int. J. Heat Mass Transf.* 158 (2020) 119992.
- [19] J. Cho, Z. Li, M. Asheghi, K.E. Goodson, Near-junction thermal management: thermal conduction in gallium nitride composite substrates, *Annu. Rev. Heat Transf.* 18 (2015) 7–45.
- [20] Y.S. Muzychka, J.R. Culham, M.M. Yovanovich, Thermal spreading resistance of eccentric heat sources on rectangular flux channels, *J. Electron. Packag.* 125 (2) (2003) 178–185.
- [21] Y.S. Muzychka, K.R. Bagnall, E.N. Wang, Thermal spreading resistance and heat source temperature in compound orthotropic systems with interfacial resistance, *IEEE Trans. Compon. Packag. Manuf. Technol.* 3 (11) (2013) 1826–1841.
- [22] A. Gholami, M. Bahrami, Thermal spreading resistance inside anisotropic plates with arbitrarily located hotspots, *J. Thermophys. Heat Transf.* 28 (4) (2014) 679–686.
- [23] A. Darwish, A.J. Bayba, H.A. Hung, Channel temperature analysis of GaN HEMTs with nonlinear thermal conductivity, *IEEE Trans. Electron. Devices* 62 (3) (2015) 840–846.
- [24] Q. Hao, Y. Xiao, Q. Chen, Determining phonon mean free path spectrum by ballistic phonon resistance within a nanoslot-patterned thin film, *Mater. Today Phys.* 10 (2019) 100126.
- [25] J.P. Freedman, J.H. Leach, E.A. Preble, Z. Sitar, R.F. Davis, J.A. Malen, Universal phonon mean free path spectra in crystalline semiconductors at high temperature, *Sci. Rep.* 3 (1) (2013) 2963.
- [26] D.-S. Tang, B.-Y. Cao, Phonon thermal transport and its tunability in GaN for near-junction thermal management of electronics: a review, *Int. J. Heat Mass Transf.* 200 (2023) 123497.
- [27] H. Bao, J. Chen, X. Gu, B. Cao, A review of simulation methods in micro/nanoscale heat conduction, *ES Energy Environ.* 1 (39) (2018) 16–55.
- [28] G. Chen, Non-fourier phonon heat conduction at the microscale and nanoscale, *Nat. Rev. Phys.* 3 (8) (2021) 555–569.
- [29] Q. Hao, H. Zhao, Y. Xiao, A hybrid simulation technique for electrothermal studies of two-dimensional GaN-on-SiC high electron mobility transistors, *J. Appl. Phys.* 121 (20) (2017) 204501.
- [30] H.-L. Li, Y. Shen, Y.-C. Hua, S.L. Sobolev, B.-Y. Cao, Hybrid Monte Carlo-diffusion studies of modeling self-heating in ballistic-diffusive regime for gallium nitride HEMTs, *J. Electron. Packag.* 145 (1) (2023) 011203.
- [31] Y. Hu, Y. Shen, H. Bao, Ultra-efficient and parameter-free computation of sub-micron thermal transport with phonon Boltzmann transport equation, *Fund. Res.* (2022) 007, doi:10.1016/j.fmre.2022.06.007.
- [32] L. Yang, Y. Jiang, Y. Zhou, Quantitatively predicting modal thermal conductivity of nanocrystalline Si by full-band Monte Carlo simulations, *Phys. Rev. B* 104 (19) (2021) 195303.
- [33] N.D. Le, B. Davier, N. Iztounene, P. Dollfus, J. Saint-Martin, Study of phonon transport across Si/Ge interfaces using full-band phonon Monte Carlo simulation, *J. Comput. Electron.* 21 (4) (2022) 744–755.
- [34] L. Chaput, J. Larroque, P. Dollfus, J. Saint-Martin, D. Lacroix, Ab initio based calculations of the thermal conductivity at the micron scale, *Appl. Phys. Lett.* 112 (3) (2018) 033104.
- [35] S. Mazumder, Boltzmann transport equation based modeling of phonon heat conduction: progress and challenges, *Annu. Rev. Heat Transf.* 24 (2022) 71–130.
- [36] Q. Hao, H. Zhao, Y. Xiao, M.B. Kronenfeld, Electrothermal studies of GaN-based high electron mobility transistors with improved thermal designs, *Int. J. Heat Mass Transf.* 116 (2018) 496–506.
- [37] Q. Hao, H. Zhao, Y. Xiao, Q. Wang, X. Wang, Hybrid electrothermal simulation of a 3-D fin-shaped field-effect transistor based on GaN nanowires, *IEEE Trans. Electron. Devices* 65 (3) (2018) 921–927.
- [38] N. Donmez, S. Graham, The impact of noncontinuum thermal transport on the temperature of AlGaN/GaN HFETs, *IEEE Trans. Electron. Devices* 61 (6) (2014) 2041–2048.
- [39] Y.-C. Hua, B.-Y. Cao, Ballistic-diffusive heat conduction in multiply-constrained nanostructures, *Int. J. Therm. Sci.* 101 (2016) 126–132.
- [40] Y.-C. Hua, B.-Y. Cao, The effective thermal conductivity of ballistic-diffusive heat conduction in nanostructures with internal heat source, *Int. J. Heat Mass Transf.* 92 (2016) 995–1003.
- [41] T. Kim, S.I. Park, C. Song, H. Lee, J. Cho, Fundamental conduction cooling limits for sub-1  $\mu\text{m}$  Ga<sub>2</sub>O<sub>3</sub> devices integrated with diamond, *Int. J. Heat Mass Transf.* 191 (2022) 122864.
- [42] Y.-C. Hua, H.-L. Li, B.-Y. Cao, Thermal spreading resistance in ballistic-diffusive regime for GaN HEMTs, *IEEE Trans. Electron. Devices* 66 (8) (2019) 3296–3301.
- [43] D.-S. Tang, G.-Z. Qin, M. Hu, B.-Y. Cao, Thermal transport properties of GaN with biaxial strain and electron-phonon coupling, *J. Appl. Phys.* 127 (3) (2020) 035102.
- [44] D.-S. Tang, B.-Y. Cao, Phonon thermal transport properties of GaN with symmetry-breaking and lattice deformation induced by the electric field, *Int. J. Heat Mass Transf.* 179 (2021) 121659.
- [45] J. Hafner, Ab-initio simulations of materials using VASP: density-functional theory and beyond, *J. Comput. Chem.* 29 (13) (2008) 2044–2078.
- [46] A. Togo, I. Tanaka, First principles phonon calculations in materials science, *Scr. Mater.* 108 (2015) 1–5.
- [47] L. Lindsay, D.A. Broido, T.L. Reinecke, First-principles determination of ultrahigh thermal conductivity of boron arsenide: a competitor for diamond? *Phys. Rev. Lett.* 111 (2) (2013) 025901.
- [48] W. Li, J. Carrete, N.A. Katcho, N. Mingo, ShengBTE: a solver of the Boltzmann transport equation for phonons, *Comput. Phys. Commun.* 185 (6) (2014) 1747–1758.
- [49] X. Ran, M. Wang, A steady-state energy-based Monte Carlo method for phonon transport with arbitrary temperature difference, *J. Heat Transf.* 144 (8) (2022) 082502.
- [50] Y.-C. Hua, B.-Y. Cao, Phonon ballistic-diffusive heat conduction in silicon nanofilms by Monte Carlo simulations, *Int. J. Heat Mass Transf.* 78 (2014) 755–759.
- [51] J.-P.M. Péraud, N.G. Hadjiconstantinou, Efficient simulation of multidimensional phonon transport using energy-based variance-reduced Monte Carlo formulations, *Phys. Rev. B* 84 (20) (2011) 205331.
- [52] J.-P.M. Péraud, N.G. Hadjiconstantinou, An alternative approach to efficient simulation of micro/nanoscale phonon transport, *Appl. Phys. Lett.* 101 (15) (2012) 153114.
- [53] B. Davier, J. Larroque, P. Dollfus, L. Chaput, S. Volz, D. Lacroix, J. Saint-Martin, Heat transfer in rough nanofilms and nanowires using full band ab initio Monte Carlo simulation, *J. Phys.* 30 (49) (2018) 495902.
- [54] D. Tang, Y. Hua, Y. Zhou, B. Cao, Thermal conductivity modeling of GaN films, *Acta Phys. Sin.* 70 (4) (2021) 045101.
- [55] R. Wu, R. Hu, X. Luo, First-principle-based full-dispersion Monte Carlo simulation of the anisotropic phonon transport in the wurtzite GaN thin film, *J. Appl. Phys.* 119 (14) (2016) 145706.
- [56] G. Chen, *Nanoscale Energy Transport and Conversion: A Parallel Treatment of Electrons, Molecules, Phonons, and Photons*, Oxford University Press, 2005.
- [57] H.-L. Li, J. Shiomi, B.-Y. Cao, Ballistic-diffusive heat conduction in thin films by phonon monte carlo method: gray medium approximation versus phonon dispersion, *J. Heat Transf.* 142 (11) (2020) 112502.
- [58] A. Majumdar, Microscale heat conduction in dielectric thin films, *J. Heat Transf.* 115 (1) (1993) 7–16.
- [59] Y. Shen, Y.-C. Hua, H.-L. Li, S.L. Sobolev, B.-Y. Cao, Spectral thermal spreading resistance of wide-bandgap semiconductors in ballistic-diffusive regime, *IEEE Trans. Electron. Devices* 69 (6) (2022) 3047–3054.
- [60] Y. Yue, X. Chen, X. Wang, Noncontact sub-10 nm temperature measurement in near-field laser heating, *ACS Nano* 5 (6) (2011) 4466–4475.
- [61] D. Huang, Q. Sun, Z. Liu, S. Xu, R. Yang, Y. Yue, Ballistic thermal transport at sub-10 nm laser-induced hot spots in GaN crystal, *Adv. Sci.* 10 (2) (2023) 2204777.
- [62] Z.-K. Liu, Y. Shen, H.-L. Li, B.-Y. Cao, Observation of ballistic-diffusive thermal transport in GaN transistors using thermoreflectance thermal imaging, arXiv preprint arXiv:2302.13975 (2023).